Title

Simulations of Friction Anisotropy on Self-Assembled Monolayers in Water

Journal

Langmuir, 38(20)

ISSN

0743-7463

Authors

Ahmad, Khurshid
Yang, Quanpeng
Martini, Ashlie

Publication Date

2022-05-24

DOI

10.1021/acs.langmuir.1c03234

Peer reviewed

Langmuir 2022
https://doi.org/10.1021/acs.langmuir.1c03234

Simulations of Friction Anisotropy on Self-assembled Monolayers in Water

Khurshid Ahmad,*,† Quanpeng Yang,‡ and Ashlie Martini‡

†*US-Pakistan Center for Advanced Studies in Energy, University of Engineering and Technology, Peshawar, 25000, Pakistan*

‡*Department of Mechanical Engineering, University of California-Merced, 5200 N. Lake Road, Merced, California 95343, United States*

E-mail: khurshid@uetpeshawar.edu.pk

Abstract

Molecular dynamics simulations were performed to study nanoscale friction on hydrophilic and hydrophobic self-assembled monolayers (SAMs) immersed in water. Sliding was simulated in two different directions to capture anisotropy due to the direction of motion relative to the inherent titled orientation of the molecules. It was shown that friction depends on both hydrophobicity and sliding direction, with the highest friction observed for sliding on hydrophobic SAM in the direction against the initial orientation of the molecules. The origins of the friction trends were analyzed by differentiating the tip-SAM and tip-water force contributions to friction. The tip-water force was higher on the hydrophilic SAM and this was shown to be due to the presence of a dense layer of water adjacent to the surface and hydrogen bonding. In contrast, the tip-SAM force was higher on the hydrophobic SAM due to a water depletion layer which enabled the tip to be closer to the SAM terminal group. The higher friction cases all exhibited greater penetration of the tip below the surface of the SAM, accommodated by further tilting and reorientation of the SAM molecules.

Introduction

Self-assembled monolayers (SAMs) have many different applications and are important for modification of surface and interface properties in micro-electro-mechanical systems (MEMS), electronic devices, and biomaterials.[1–4] SAMs can modify surface properties like adhesion,[5–7] liquid repellency,[8–10] and various tribological characteristics.[6,7,9] SAMs can also be used for lubrication and protection of MEMS surfaces and interfaces.[11] The properties of SAMs, such as contact angle, adhesion, and friction, are directly correlated to their molecular features, e.g., chain length and terminal group chemistry.[12,13] Therefore, understanding, predicting, and controlling the properties of SAMs is important to their use in a variety of applications.[12]

Various experimental techniques, such as X-ray diffraction,[14] infrared spectroscopy,[15] scanning force microscopy,[16,17] interfacial force microscopy[18] and atomic force microscopy (AFM)[19–21] have been used to study the structural and mechanical properties of SAMs. Particularly, AFM has been used to characterize friction on SAMs using a wide range of different tips (Si_3N_4, Au, and -CH_3 or -OH terminated SAMs),[16,22–24] substrates (Au, Si),[25–29] and environments (ethanol, hexadecane, water, humid air, and dry air).[26,30–35] The sliding systems studied using AFM have included SAM-SAM,[36] tip-SAM, and SAM-tip-water[26,35] combinations.

Experimental work has been complemented by molecular dynamics (MD) simulations of SAMs.[11,35,37–41] MD simulation is a powerful tool to study nanoscale interfaces because it can precisely control the factors affecting friction, such as sliding direction, load, and velocity. Friction has been shown to be higher on hydrophilic vs. hydrophobic SAMs.[35,42] In addition, the presence of water molecules can change the magnitude of friction force on hydrophilic SAM.[26,35,41,42] For a hydrophilic silicon nitride tip or hydrophilic SAM sliding on hydrophilic SAM, water lowers friction due to layering of the water molecules between the sliding surfaces, thus providing lubrication.[26,41] However, when a carbon tip is sliding over hydrophilic SAM, water increases friction due to hydrogen bonding (H-bonding) between the water molecules and the terminal -OH groups on the SAM, thus offering additional resistance

to sliding.[35]

Both experiments and simulations have reported that friction on SAMs is anisotropic,[11,39,43] where anisotropy refers to the observation that friction is dependent on the sliding direction. Some studies have attributed friction anisotropy to the tilt angle (with respect to the surface-normal direction) and the orientation angle (with respect to the sliding direction) of the SAM molecules.[11,37,43] MD simulations of SAM-SAM sliding in vacuum reported higher friction when the SAMs were aligned in the direction of sliding.[44] The same study proposed that subtle structural variations could affect friction due to steric constraints leading to different van der Waals interactions between the terminal groups and an interacting surface.[44] Although friction on SAMs in water has been studied with MD simulations,[35,45] friction anisotropy on SAMs in a liquid environment has not been modeled.

In this work, we performed MD simulations of atomic scale friction between a nanoscale AFM probe and alkanethiol monolayers terminated with -CH_3 (hydrophobic) or -OH (hydrophilic) groups in the presence of water to study friction anisotropy. In our model, hydrophilic and hydrophobic SAMs with the same chain length were positioned next to each other on a gold substrate in the model system such that the friction force could be measured by sliding the tip from one type of SAM to the other along a single scan line. The model was designed to mimic previous AFM experiments in which SAM friction was studied by measuring friction of multiple SAMs on the same sample. [22,29,35,46] In the simulations, friction anisotropy on both hydrophilic and hydrophobic SAMs was analyzed across a range of normal loads. The friction trends were analyzed in terms of the force between the tip and SAMs (tip-SAM force) and the tip and water (tip-water force), layering and position of water adjacent to the SAM terminal groups, number of H-bonds formed between the water and the hydrophilic SAM molecules, SAM tilt and orientation angles, and the depth of penetration of the tip into the SAMs while sliding.

Methods and Models

As shown in Fig. 1a, the model SAMs consisted of hydrophilic 11-mercapto-1-undecanol ($-S(CH_2)_{11}OH$) and hydrophobic 1-dodecanethiol ($-S(CH_2)_{11}CH_3$), respectively. The model was created by arranging 120 molecules of each type on an approximately 1.2 nm thick atomically flat Au (111) surface. A tip with hemispherical apex of radius 1.5 nm composed of carbon atoms in a diamond crystallographic lattice was placed above the SAMs surface. Although the model tip radius is smaller than those used in AFM experiments,[35,46–48] it is consistent with previous MD simulations that modeled very small tips due to computational limitations.[35,38,49,50] Since only the apex of the tip was explicitly modeled in the simulations, the stiffness of the remainder of the tip and cantilever was captured by connecting the model tip apex to a virtual atom through a harmonic spring.[49–53] The spring stiffness was set to 1.6 N/m in the x- and y-directions, consistent with previous modeling studies and comparable to the stiffness of cantilevers used for friction force microscopy.[54] The space above the SAMs and the surrounding the tip was filled with water with a density of approximately 1.0 g/cm^3. Periodic boundary conditions were applied to the simulation box. The model was constructed using Avogadro 1.2[55] and Moltemplate[56] tools, while Ovito[57] was used for the visualization of the models. All simulations were performed using LAMMPS (Large-scale Atomic/Molecular Massively Parallel Simulator).[58]

The details of model construction were described in our previous studies.[35,59,60] Briefly, the water molecules were modeled using the extended simple point charge potential (SPC/E).[61] The sulfur-gold interactions were modeled using the Morse potential[62,63] while the Lorentz-Berthelot mixing rules [64] and the Lennard-Jones potential [65] were used for all other long-range interactions. The united atom model [12] was used for modeling -CH_2 and -CH_3. The embedded atom method and an adaptive intermolecular reactive empirical bond order (AIREBO) potential were used for modeling the interactions within the gold substrate and the tip, respectively. During simulations, the bottom 0.1 nm of the gold substrate was fixed and the top few layers of tip atoms were treated as a rigid body.

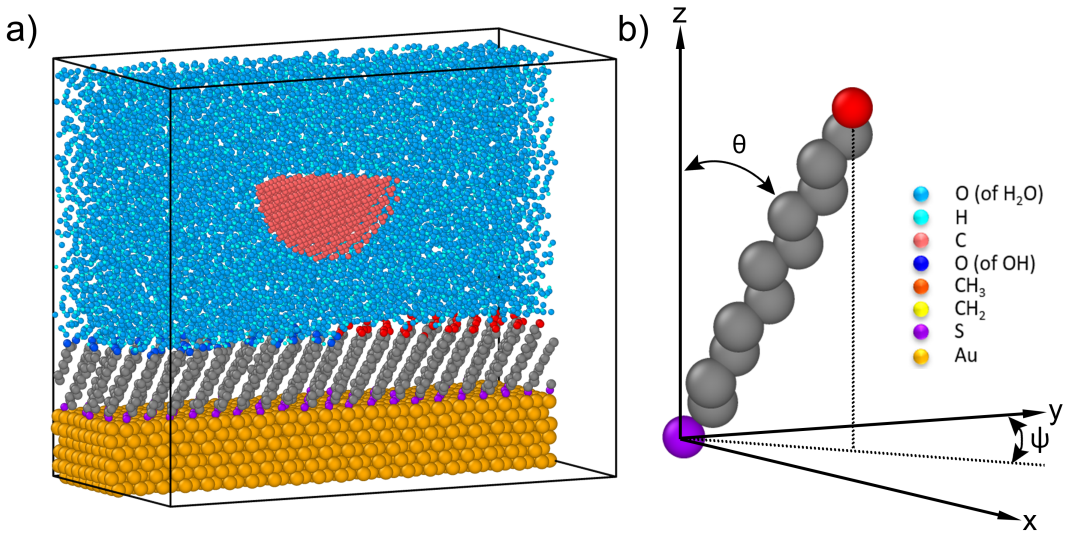

Figure 1: (a) Snapshot of half of the equilibrated simulation model and (b) schematic illustration the tilt and orientation angles of a SAM molecule. θ is the tilt angle of the molecules with respect to the surface-normal (z-direction) while ψ is the orientation angle of the SAMs relative to the sliding direction (y-direction).

The system was equilibrated in the NPT ensemble at 0.1 MPa and 300 K, and then in the NVT ensemble at 300 K, for 50 ps each. The Nosé-Hoover thermostat and barostat were used with damping factors of 0.1 and 1.0 ps, respectively. The SAM molecules exhibited tilt and orientation angles, as defined in Fig. 1b. At equilibrium, the average tilt angle with respect to surface-normal was 28.6±4.0° for the hydrophilic SAM and 30.0±2.3° for the hydrophobic SAM, both of which are close to the value (33.7±0.3°) measured for $-S(CH_2)_{11}CH_3$ chains using X-ray diffraction.[14] The equilibrium orientation angles (with respect to sliding direction) for the hydrophilic and hydrophobic SAMs were 64.4±10.2° and 64.0±4.4°, respectively.

After equilibration, normal loads between 0.4 and 1.0 nN were applied on the tip, followed by another system equilibration in an NVT ensemble until the z-position of the tip reached steady state. Generally, steady state was achieved in 3.5 to 4.5 ns. The corresponding maximum contact pressures ranged from 0.24 to 0.39 GPa, estimated based on the Hertz contact model. To simulate sliding, the virtual atom was dragged with a velocity of 2 m/s over the SAMs surface in either the positive (forward) or negative (backward) y-direction.

The tip motion in both the x- and y-directions was limited by the harmonic spring and the rotation of the top few layers of tip atoms was restricted. The z-axis is orthogonal to the Au (111) plane while the sliding direction (y-axis) is orthogonal to the (110) plane.

The friction force was calculated as the force on the spring in the direction opposite to the sliding. All friction simulations were repeated six times, realized by allowing the tip to pass through the periodic boundaries of the simulation box six times, each referred to as a cycle. Next, the friction force was averaged over five sliding cycles, excluding the static friction exhibited in the first cycle. The results were then averaged again over lateral distances of 1.5 to 3.5 nm for hydrophilic SAM and 6.5 to 8.5 nm for hydrophobic SAM. These lateral distance ranges were chosen to minimize the effects of the boundaries between the two SAMs.

Results and Discussion

The tip was slid forward and backward over the SAMs immersed in water. Representative plots of friction force versus lateral distance in both sliding directions at a load of 0.8 nN are shown in Fig. 2. Here, forward refers to the positive y-direction while backward refers to the negative y-direction.

The average friction (for cycles 2 through 6) as a function of load is shown in Fig. 3. Friction force generally increased with increasing load and the friction coefficient was calculated from linear fits to the data. The friction force and coefficient were the largest for hydrophobic SAM in the backward sliding case. The lowest friction force was observed for forward sliding on the hydrophobic SAM and the lowest friction coefficient was found for the hydrophilic SAM with backward sliding. These results show that both hydrophobicity and sliding direction affect the friction on SAMs.

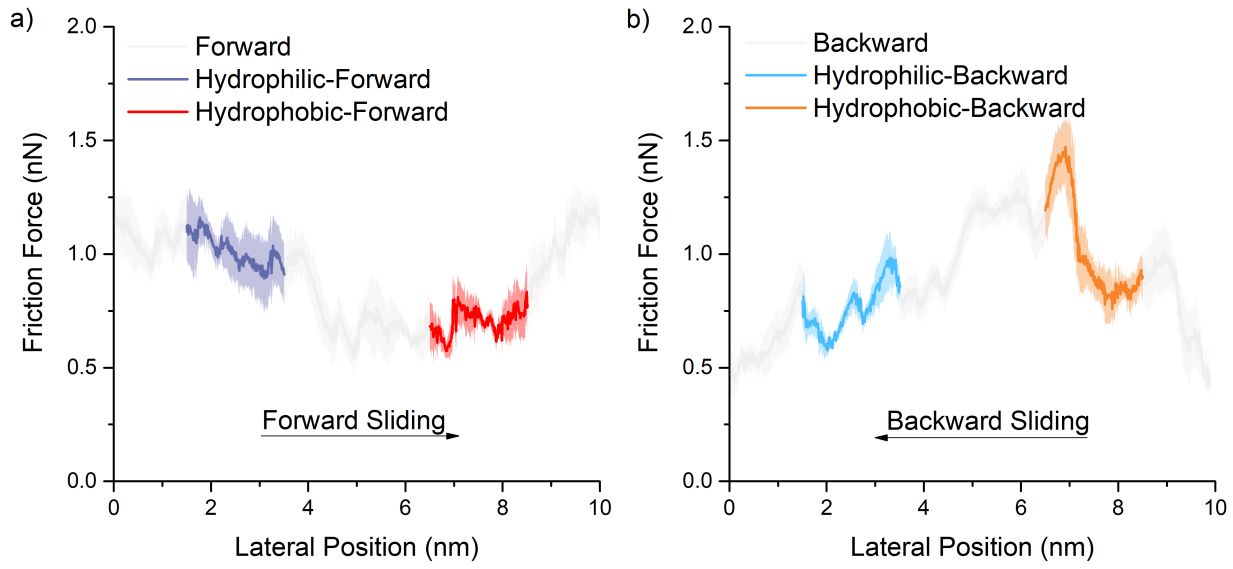

Figure 2: Friction force on the SAMs in water as a function of the lateral position of the tip sliding in the (a) forward and (b) backward directions sliding over the hydrophilic (1.5-3.5 nm, purple and blue) and hydrophobic (6.5-8.5 nm red and orange) SAMs with a normal load of 0.8 nN. The gray regions are the friction when the tip is near the boundary between the hydrophobic and hydrophilic SAMs. This data is excluded from results shown subsequently in the paper. The solid lines show the friction force averaged over the last five sliding cycles, while the light color regions are the standard error.

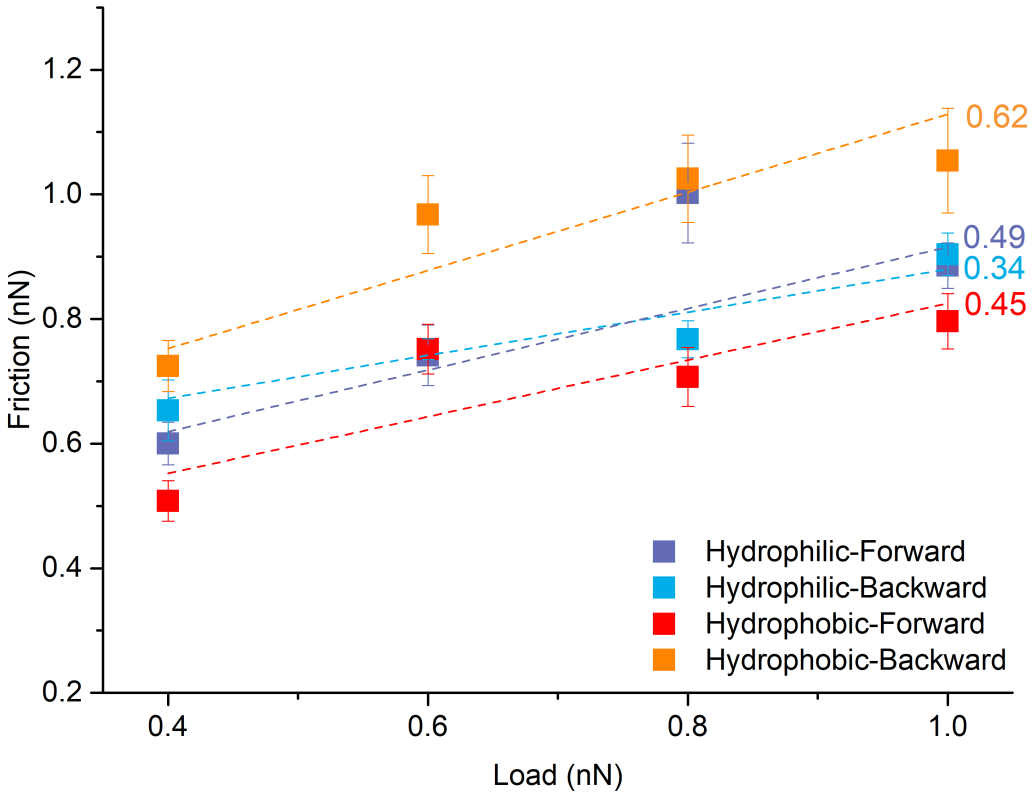

Figure 3: Average friction as a function of load for hydrophilic and hydrophobic SAMs with sliding in the forward and backward directions. Forward is defined as sliding in the positive y-direction and backward as sliding in the negative y-direction. The error bars show standard error over five sliding cycles. Dashed lines show linear fits to the data where the slope is the friction coefficient, value given to the right of the 1.0 nN data point for each case.

Both tip-SAM and tip-water forces contribute to the total friction,[35] so these forces are analyzed separately, as shown in Fig. 4. We first consider the force between the tip and the water. As shown in Fig. 4a, the tip-water force is significantly higher on the hydrophilic SAM than on the hydrophobic SAM for sliding in either direction and at any load.

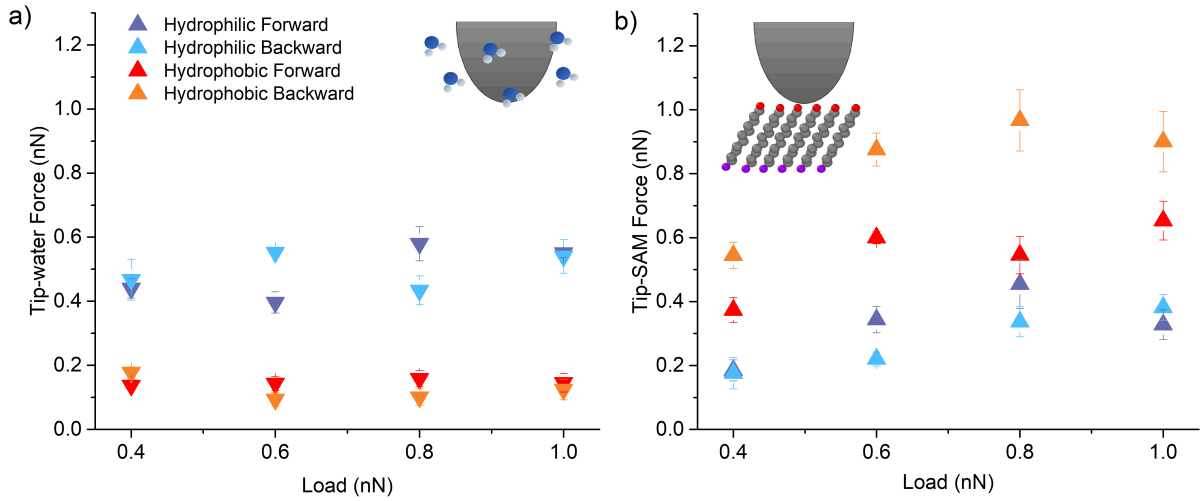

Figure 4: Contributions of the lateral force between (a) the tip and water and (b) the tip and SAM molecules to the total friction force. The error bars show standard error over five sliding cycles.

The larger tip-water force on the hydrophilic SAM can be attributable to a dense layer of water near the SAM surface.[26,35,41] The presence of this layer was confirmed by calculating the radial distribution function (RDF) for the distance between the terminal group of the SAM molecules and the O atom in the water molecules, as shown in Fig. 5. For both hydrophobic and hydrophilic SAMs, the first peak in the RDF corresponding to the first layer of water adjacent to the SAM terminal groups. For the hydrophobic SAM, the RDF peak suggests that the water layer is further from the surface ($\sim$0.38 nm), indicating the existence of a depletion layer.[66] The depletion layer can explain the relatively small tip-water force on the hydrophobic SAM. In contrast, the RDF peak for the hydrophilic SAM is at $\sim$0.28 nm, indicating a dense layer of water adjacent to the SAM surface. The tip interacts with the water in this dense layer as it slides, which increases friction on the hydrophilic surface.

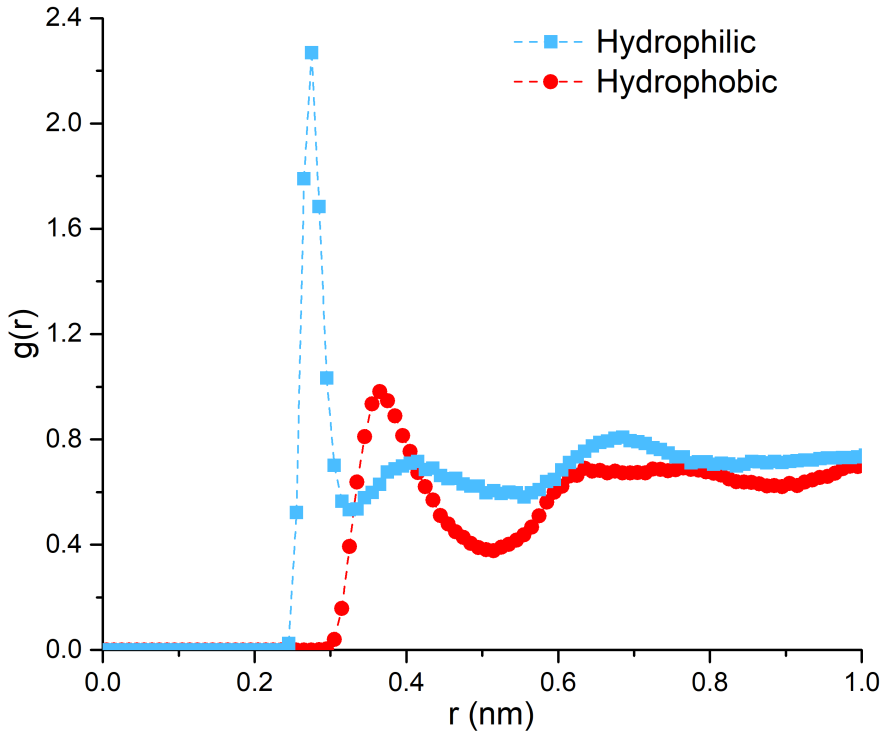

Figure 5: Distribution of distances, g(r), between the water and the terminal group on the hydrophilic (blue line) and hydrophobic (red line) SAMs. The peak at 0.28 nm for the hydrophilic SAM indicates a dense water layer adjacent to the surface while water is repelled from the hydrophobic SAM creating a depletion layer.

We repeated the RDF calculation for both hydrophilic SAM-water and hydrophobic SAM-water distances at all loads and the same first peak position was observed at all loads (Figure S1). Note that these RDFs correspond to the distance between the SAMs and water. We also calculated the RDF for the O-O distance between water molecules, to evaluate the possibility of an ice-like structure forming between the tip and SAM.[45] However, there was no additional peak indicative of ice-like structure (Figure S2), likely because of the relatively low pressure in these simulations and the small tip size that confines only a few water molecules at any given time.

H-bonding may also contribute to the tip-water force trends since the -OH tails of hydrophilic SAM not only interact with each other through H-bonding [37,41,42] but also form

H-bonds with water molecules in their vicinity.[35] The hydrophilic SAM-water H-bonds are broken during sliding, contributing to friction. To quantify this effect, first, H-bonds were identified based on the distances and angles between atoms using previously established criteria.[35,67] Then, the number of bonds broken per sliding cycle was calculated as the difference between the average number of hydrophilic SAM–water H-bonds when the tip was sliding on the hydrophilic SAM (distances 1.5 to 3.5 nm) and the average number of hydrophilic SAM–water H-bonds when the tip was sliding on the hydrophobic SAM (distances 6.5 to 8.5 nm). As shown in Fig. 6, approximately 6 to 15 H-bonds were broken per sliding cycle, at various normal loads ranging from 0.4 to 1.0 nN. The extra energy required to break H-bonds when sliding on the hydrophilic SAM contributes to higher tip-water force.

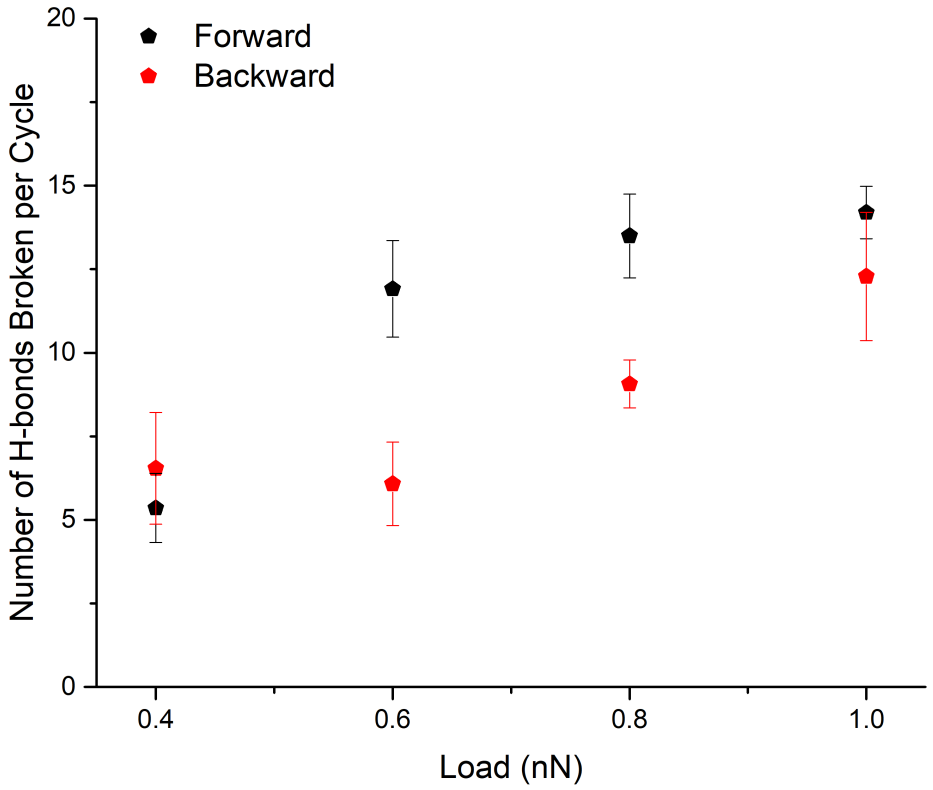

Figure 6: Number of hydrophilic SAM–water H-bonds broken per cycle as a function of load. The error bars show standard error over five sliding cycles.

Friction is also due to tip-SAM forces. As shown in Fig. 4b, the tip-SAM force is higher

on the hydrophobic SAM than the hydrophilic SAM for sliding in both directions. This can be partially explained by the RDFs in Fig. 5, since the lack of water in the depletion layer means the tip is closer to the SAMs and there is larger tip-SAM force.[68]

Previous experiments as well as MD simulation studies have reported that the friction force on SAMs can be attributed to plowing,[36] which occurs due to the penetration of tip into the SAM.[38,68] To quantify this, we tracked the position of the tip in the surface-normal direction during sliding. Penetration depth was defined as the average distance between the bottom-most atoms of the tip apex during sliding and the equilibrium positions of the terminal groups of the hydrophilic or hydrophobic SAM molecules. The average depth of penetration calculated at various normal loads is reported in Fig. 7. Consistent with the tip-SAM force trends in Fig. 4b, the penetration depth is the largest for the hydrophobic SAM during backward sliding.

The penetration depth trends may be attributed to differences in the compression of the SAM chains[36,68,69] and reorientation of the chains that affects packing and density.[39,40] Reorientation was quantified by the average tilt and orientation angles of SAMs at each load, shown in Fig. 8. Friction anisotropy has been attributed to tilt angles in previous research[11,37] and here is shown to explain the tip-SAM contribution to friction. Although the tilt angles on both SAMs are around 30° at equilibrium, they increase once sliding starts and reach a larger steady state value after the first cycle (see Figure S3). This indicates that the motion of the tip pushes the molecules down toward the substrate. The average steady-state tilt angles are shown in Fig. 8a and it can be seen that the tilt angle is consistently higher for the hydrophobic than the hydrophilic SAM. This is consistent with the greater penetration of the tip into the SAMs in Fig. 7 and the higher tip-SAM force of the hydrophobic SAM.

Similar trends are exhibited by the orientation angles. The average steady-state orientation angles for the two SAMs as a function of load are shown in Fig. 8b. Like the tilt angles, the orientation angles are larger on the hydrophobic SAM, indicating that SAM chains are pushed further out to the sides and away from the sliding direction. There are also a sta-

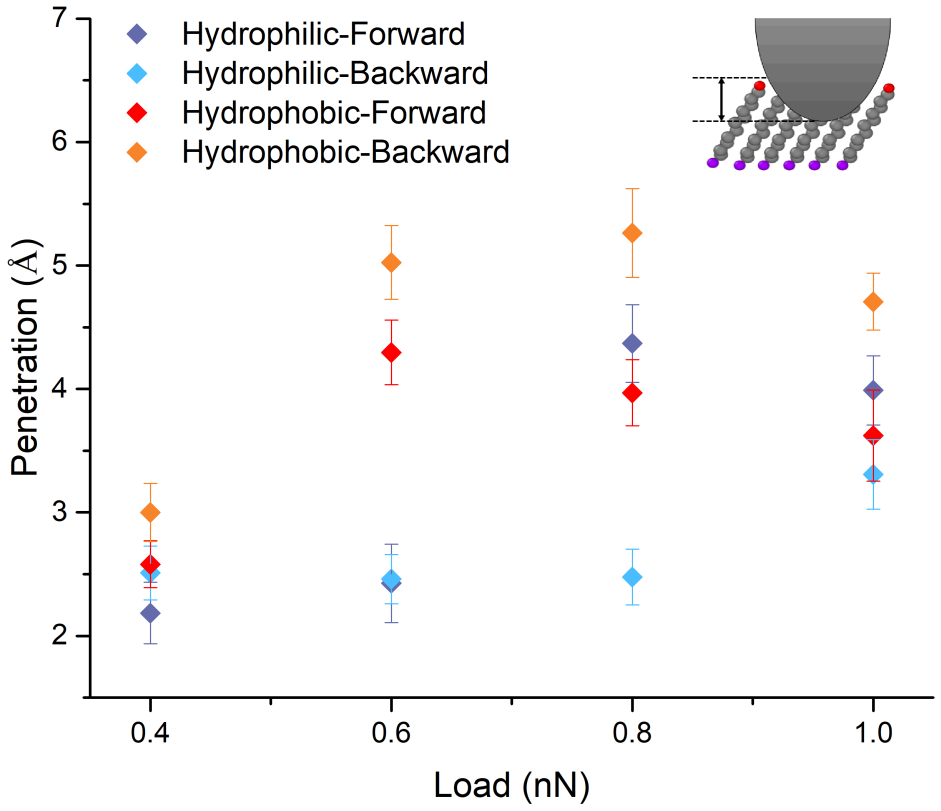

Figure 7: Penetration depth as a function of load for hydrophilic and hydrophobic SAMs sliding in the forward and backward directions. The error bars show standard error over five sliding cycles.

tistically significant differences between the orientation angles in the forward and backward directions on hydrophobic SAM at several loads. This can be explained by considering the evolution of orientation angle with cycle (see Figure S4). In the forward sliding case, the orientation angle starts (at cycle 0) around 65° and ends up around 50°. However, for backward sliding, this same starting configuration corresponds to 115° orientation (with respect to the negative y-axis). Then, during steady-state sliding in the backward direction, the orientation angle is a little over 60°. These results are consistent with the trends exhibited by the depth of penetration as a function of cycle (Figure S5), indicating that the tip initially had to reorient the chains to slide backward, which enabled more penetration into the

SAM surface, thereby increasing friction. These results indicate that the tip is able to move down into the SAM when the chains are tilted further from the surface-normal direction and pushed out to the side of the sliding path by the tip. The energy required to tilt the chains and push them aside contributes to higher friction.

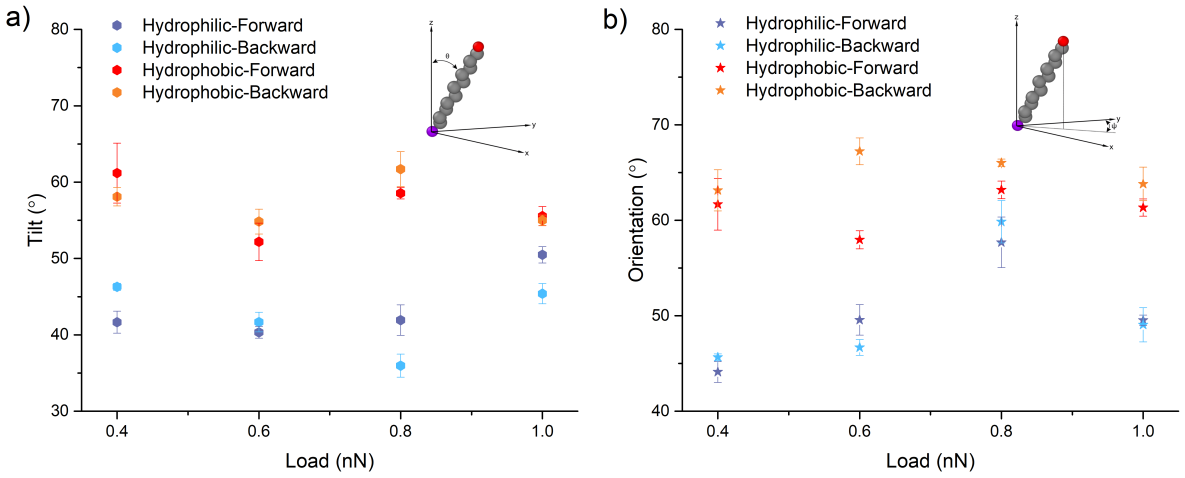

Figure 8: (a) Tilt and (b) orientation angles as a function of load for hydrophilic and hydrophobic SAMs with sliding in the forward and backward directions. The angles are defined as shown in Fig. 1b. The error bars show standard error over five sliding cycles.

Conclusions

We studied the friction anisotropy on hydrophilic and hydrophobic SAMs immersed in water for sliding in two opposite directions. It was found that both hydrophobicity and sliding direction affect friction. Multiple mechanisms, including H-bonding between SAM and water molecules, tip-SAM interactions, the depth of tip penetration into SAM molecules, and the SAM molecule orientation and tilt angles, were analyzed to identify mechanisms underlying the observed friction trends. It was found that the tip-water force was dominant for the hydrophilic SAM and there was no significant direction dependence. However, for hydrophobic SAM, the friction was due mostly to tip-SAM force and direction dependence was observed. The water depletion layer on the hydrophobic SAM caused stronger interactions between

the tip and SAM, such that the tip had to push the SAM downward (increased tilt angle) and to the side (increased orientation angle) to slide. The energy required to reorient the SAMs increased the overall friction force. Overall, the results show that friction on SAMs in water is determined by both tip-SAM and tip-water force, and that both of these are affected by SAM terminal group chemistry and sliding direction. The findings also demonstrate that a key energy dissipation mechanism for SAMs is associated with their inherently tilted configuration relative to the surface and the ability to change orientation in response to sliding.

Acknowledgement

KA acknowledges the support of Institute of International Education (IIE) and United States Education Foundation in Pakistan (USEFP) through Fulbright Scholar Program and University of Engineering and Technology Peshawar, Pakistan. AM and QY acknowledge the support of the National Science Foundation through Grant #CHE 1808213. The simulations were in part run using the Extreme Science and Engineering Discovery Environment (XSEDE), which is supported by National Science Foundation Grant ACI-1548562.

Supporting Information Available

Supporting Information. The supporting information contains additional analysis of SAM-water and O-O (in water) radial distribution functions, tilt and orientation angles of SAMs vs cycle, depth of penetration vs cycle.

References

(1) Mougin, K.; Haidara, H. *Fundamentals of Friction and Wear*; Springer, 2007; pp 619–645.

(2) Hasan, A.; Pandey, L. *Nanobiomaterials*; Elsevier, 2018; pp 137–178.

(3) Singh, M.; Kaur, N.; Comini, E. The role of self-assembled monolayers in electronic devices. *Journal of Materials Chemistry C* **2020**, *8*, 3938–3955.

(4) Love, J. C.; Estroff, L. A.; Kriebel, J. K.; Nuzzo, R. G.; Whitesides, G. M. Self-assembled monolayers of thiolates on metals as a form of nanotechnology. *Chemical reviews* **2005**, *105*, 1103–1170.

(5) Elinski, M. B.; Menard, B. D.; Liu, Z.; Batteas, J. D. Adhesion and friction at graphene/self-assembled monolayer interfaces investigated by atomic force microscopy. *The Journal of Physical Chemistry C* **2017**, *121*, 5635–5641.

(6) Baker, M.; Li, J. The influence of an OTS self-assembled monolayer on the wear-resistant properties of polysilicon based MEMS. *Surface and Interface Analysis: An International Journal devoted to the development and application of techniques for the analysis of surfaces, interfaces and thin films* **2006**, *38*, 863–867.

(7) Chandross, M.; Grest, G. S.; Stevens, M. J. Friction between alkylsilane monolayers: Molecular simulation of ordered monolayers. *Langmuir* **2002**, *18*, 8392–8399.

(8) Whitesides, G. M.; Laibinis, P. E. Wet chemical approaches to the characterization of organic surfaces: self-assembled monolayers, wetting, and the physical-organic chemistry of the solid-liquid interface. *Langmuir* **1990**, *6*, 87–96.

(9) DePalma, V.; Tillman, N. Friction and wear of self-assembled trichlorosilane monolayer films on silicon. *Langmuir* **1989**, *5*, 868–872.

(10) Ahmad, K.; Zhao, X.; Pan, Y. Effect of surface morphology on measurement and interpretation of boundary slip on superhydrophobic surfaces. *Surface and Interface Analysis* **2017**, *49*, 594–598.

(11) Jabbarzadeh, A. Friction anisotropy and asymmetry in self assembled monolayers. *Tribology International* **2016**, *102*, 600–607.

(12) Jiang, S. Molecular simulation studies of self-assembled monolayers of alkanethiols on Au (111). *Molecular physics* **2002**, *100*, 2261–2275.

(13) Bain, C. D.; Evall, J.; Whitesides, G. M. Formation of monolayers by the coadsorption of thiols on gold: variation in the head group, tail group, and solvent. *Journal of the American Chemical Society* **1989**, *111*, 7155–7164.

(14) Fenter, P.; Eberhardt, A.; Liang, K. S.; Eisenberger, P. Epitaxy and chainlength dependent strain in self-assembled monolayers. *The Journal of chemical physics* **1997**, *106*, 1600–1608.

(15) Stole, S. M.; Porter, M. D. In situ infrared external reflection spectroscopy as a probe of the interactions at the liquid-solid interface of long-chain alkanethiol monolayers at gold. *Langmuir* **1990**, *6*, 1199–1202.

(16) Li, L.; Yu, Q.; Jiang, S. Quantitative measurements of frictional properties of n-alkanethiols on Au (111) by scanning force microscopy. *The Journal of Physical Chemistry B* **1999**, *103*, 8290–8295.

(17) McDermott, M. T.; Green, J.-B. D.; Porter, M. D. Scanning force microscopic exploration of the lubrication capabilities of n-alkanethiolate monolayers chemisorbed at gold: structural basis of microscopic friction and wear. *Langmuir* **1997**, *13*, 2504–2510.

(18) Kiely, J. D.; Houston, J. E.; Mulder, J. A.; Hsung, R. P.; Zhu, X. Adhesion, deformation and friction for self-assembled monolayers on Au and Si surfaces. *Tribology Letters* **1999**, *7*, 103–107.

(19) Engelkes, V. B.; Frisbie, C. D. Simultaneous nanoindentation and electron tunneling

through alkanethiol self-assembled monolayers. *The journal of physical chemistry B* **2006**, *110*, 10011–10020.

(20) Gojzewski, H.; Kappl, M.; Ptak, A. Effect of the chain length and temperature on the adhesive properties of alkanethiol self-assembled monolayers. *Langmuir* **2017**, *33*, 11862–11868.

(21) Lee, D. H.; Oh, T.; Cho, K. Combined effect of chain length and phase state on adhesion/friction behavior of self-assembled monolayers. *The Journal of Physical Chemistry B* **2005**, *109*, 11301–11306.

(22) Noy, A.; Vezenov, D. V.; Lieber, C. M. Chemical force microscopy. *Annual Review of Materials Science* **1997**, *27*, 381–421.

(23) Fujihira, M.; Tani, Y.; Furugori, M.; Akiba, U.; Okabe, Y. Chemical force microscopy of self-assembled monolayers on sputtered gold films patterned by phase separation. *Ultramicroscopy* **2001**, *86*, 63–73.

(24) van der Vegte, E. W.; Hadziioannou, G. Scanning force microscopy with chemical specificity: an extensive study of chemically specific tip- surface interactions and the chemical imaging of surface functional groups. *Langmuir* **1997**, *13*, 4357–4368.

(25) Brewer, N. J.; Foster, T. T.; Leggett, G. J.; Alexander, M. R.; McAlpine, E. Comparative investigations of the packing and ambient stability of self-assembled monolayers of alkanethiols on gold and silver by friction force microscopy. *The Journal of Physical Chemistry B* **2004**, *108*, 4723–4728.

(26) Li, L.; Chen, S.; Jiang, S. Nanoscale frictional properties of mixed alkanethiol self-assembled monolayers on Au (111) by scanning force microscopy: humidity effect. *Langmuir* **2003**, *19*, 666–671.

(27) Takano, H.; Kenseth, J. R.; Wong, S.-S.; O'Brien, J. C.; Porter, M. D. Chemical and biochemical analysis using scanning force microscopy. *Chemical Reviews* **1999**, *99*, 2845–2890.

(28) Tocha, E.; Schönherr, H.; Vancso, G. J. Quantitative nanotribology by AFM: a novel universal calibration platform. *Langmuir* **2006**, *22*, 2340–2350.

(29) Chong, K. S.; Sun, S.; Leggett, G. J. Measurement of the kinetics of photo-oxidation of self-assembled monolayers using friction force microscopy. *Langmuir* **2005**, *21*, 3903–3909.

(30) Clear, S. C.; Nealey, P. F. Chemical force microscopy study of adhesion and friction between surfaces functionalized with self-assembled monolayers and immersed in solvents. *Journal of colloid and interface science* **1999**, *213*, 238–250.

(31) López-Santos, C.; Yubero, F.; Cotrino, J.; González-Elipe, A. Lateral and in-depth distribution of functional groups on diamond-like carbon after oxygen plasma treatments. *Diamond and related materials* **2011**, *20*, 49–56.

(32) Te Riet, J.; Smit, T.; Gerritsen, J. W.; Cambi, A.; Elemans, J. A.; Figdor, C. G.; Speller, S. Molecular friction as a tool to identify functionalized alkanethiols. *Langmuir* **2010**, *26*, 6357–6366.

(33) Wilbur, J. L.; Biebuyck, H. A.; MacDonald, J. C.; Whitesides, G. M. Scanning force microscopies can image patterned self-assembled monolayers. *Langmuir* **1995**, *11*, 825–831.

(34) Vezenov, D. V.; Noy, A.; Rozsnyai, L. F.; Lieber, C. M. Force titrations and ionization state sensitive imaging of functional groups in aqueous solutions by chemical force microscopy. *Journal of the American Chemical Society* **1997**, *119*, 2006–2015.

(35) Yang, Q.; Nanney, W.; Hu, X.; Ye, T.; Martini, A. Nanoscale Friction of Hydrophilic and Hydrophobic Self-Assembled Monolayers in Water. *Tribology Letters* **2020**, *68*, 1–9.

(36) Flater, E. E.; Ashurst, W. R.; Carpick, R. W. Nanotribology of octadecyltrichlorosilane monolayers and silicon: Self-mated versus unmated interfaces and local packing density effects. *Langmuir* **2007**, *23*, 9242–9252.

(37) Zhang, L.; Leng, Y.; Jiang, S. Tip-based hybrid simulation study of frictional properties of self-assembled monolayers: effects of chain length, terminal group, scan direction, and scan velocity. *Langmuir* **2003**, *19*, 9742–9747.

(38) Leng, Y.; Jiang, S. Atomic indentation and friction of self-assembled monolayers by hybrid molecular simulations. *The Journal of Chemical Physics* **2000**, *113*, 8800–8806.

(39) Ramin, L.; Jabbarzadeh, A. Effect of compression on self-assembled monolayers: a molecular dynamics study. *Modelling and Simulation in Materials Science and Engineering* **2012**, *20*, 085010.

(40) Tupper, K. J.; Brenner, D. W. Compression-induced structural transition in a self-assembled monolayer. *Langmuir* **1994**, *10*, 2335–2338.

(41) Zhang, L.; Jiang, S. Molecular simulation study of nanoscale friction for alkyl monolayers on Si (111). *The Journal of Chemical Physics* **2002**, *117*, 1804–1811.

(42) Zhang, L.; Jiang, S. Molecular simulation study of nanoscale friction between alkyl monolayers on Si (111) immersed in solvents. *The Journal of chemical physics* **2003**, *119*, 765–770.

(43) Liley, M.; Gourdon, D.; Stamou, D.; Meseth, U.; Fischer, T.; Lautz, C.; Stahlberg, H.; Vogel, H.; Burnham, N.; Duschl, C. Friction anisotropy and asymmetry of a compliant monolayer induced by a small molecular tilt. *Science* **1998**, *280*, 273–275.

(44) Ramin, L.; Jabbarzadeh, A. Frictional properties of two alkanethiol self assembled monolayers in sliding contact: Odd-even effects. *The Journal of chemical physics* **2012**, *137*, 174706.

(45) Ramin, L.; Jabbarzadeh, A. Effect of water on structural and frictional properties of self assembled monolayers. *Langmuir* **2013**, *29*, 13367–13378.

(46) Noy, A.; Frisbie, C. D.; Rozsnyai, L. F.; Wrighton, M. S.; Lieber, C. M. Chemical force microscopy: exploiting chemically-modified tips to quantify adhesion, friction, and functional group distributions in molecular assemblies. *Journal of the American Chemical Society* **1995**, *117*, 7943–7951.

(47) Hu, L.; Wang, J.; Hou, K.; Yang, S. Robust ultralow friction between graphene and octadecyltrichlorosilane self-assembled monolayers. *Applied Surface Science* **2019**, *475*, 389–396.

(48) Gourdon, D.; Burnham, N. A.; Kulik, A.; Dupas, E.; Oulevey, F.; Gremaud, G.; Stamou, D.; Liley, M.; Dienes, Z.; Vogel, H. The dependence of friction anisotropies on themolecular organisation of LB films as observed by AFM. *Tribology Letters* **1997**, *3*, 317–324.

(49) Li, Q.; Dong, Y.; Perez, D.; Martini, A.; Carpick, R. W. Speed dependence of atomic stick-slip friction in optimally matched experiments and molecular dynamics simulations. *Physical review letters* **2011**, *106*, 126101.

(50) Dong, Y.; Li, Q.; Martini, A. Molecular dynamics simulation of atomic friction: A review and guide. *Journal of Vacuum Science & Technology A: Vacuum, Surfaces, and Films* **2013**, *31*, 030801.

(51) Leng, Y.; Jiang, S. Spanning time scales in dynamic simulations of atomic-scale friction. *Tribology Letters* **2001**, *11*, 111–115.

(52) Smith, R.; Mulliah, D.; Kenny, S. D.; McGee, E.; Richter, A.; Gruner, M. Stick slip and wear on metal surfaces. *Wear* **2005**, *259*, 459–466.

(53) Kim, W. K.; Falk, M. L. Atomic-scale simulations on the sliding of incommensurate surfaces: the breakdown of superlubricity. *Physical Review B* **2009**, *80*, 235428.

(54) Carpick, R. W.; Ogletree, D. F.; Salmeron, M. Lateral stiffness: a new nanomechanical measurement for the determination of shear strengths with friction force microscopy. *Applied Physics Letters* **1997**, *70*, 1548–1550.

(55) Hanwell, M. D.; Curtis, D. E.; Lonie, D. C.; Vandermeersch, T.; Zurek, E.; Hutchison, G. R. Avogadro: an advanced semantic chemical editor, visualization, and analysis platform. *Journal of cheminformatics* **2012**, *4*, 1–17.

(56) Jewett, A. I.; Zhuang, Z.; Shea, J.-E. Moltemplate a coarse-grained model assembly tool. *Biophysical Journal* **2013**, *104*, 169a.

(57) Stukowski, A. Visualization and analysis of atomistic simulation data with OVITO–the Open Visualization Tool. *Modelling and Simulation in Materials Science and Engineering* **2009**, *18*, 015012.

(58) Plimpton, S. Fast parallel algorithms for short-range molecular dynamics. *Journal of computational physics* **1995**, *117*, 1–19.

(59) Hu, X.; Nanney, W.; Umeda, K.; Ye, T.; Martini, A. Combined experimental and simulation study of amplitude modulation atomic force microscopy measurements of self-assembled monolayers in water. *Langmuir* **2018**, *34*, 9627–9633.

(60) Hu, X.; Yang, Q.; Ye, T.; Martini, A. Simulation of Subnanometer Contrast in Dynamic Atomic Force Microscopy of Hydrophilic Alkanethiol Self-Assembled Monolayers in Water. *Langmuir* **2020**, *36*, 2240–2246.

(61) Berendsen, H.; Grigera, J.; Straatsma, T. The missing term in effective pair potentials. *Journal of Physical Chemistry* **1987**, *91*, 6269–6271.

(62) Mahaffy, R.; Bhatia, R.; Garrison, B. J. Diffusion of a butanethiolate molecule on a Au {111} surface. *The Journal of Physical Chemistry B* **1997**, *101*, 771–773.

(63) Sung, I.-H.; Kim, D.-E. Molecular dynamics simulation study of the nano-wear characteristics of alkanethiol self-assembled monolayers. *Applied Physics A* **2005**, *81*, 109–114.

(64) Allen, M. P.; Tildesley, D. J. *Computer simulation of liquids*; Oxford university press, 2nd Edition, 2017; pp 1–626.

(65) Ong, W.-L.; Majumdar, S.; Malen, J. A.; McGaughey, A. J. Coupling of organic and inorganic vibrational states and their thermal transport in nanocrystal arrays. *The Journal of Physical Chemistry C* **2014**, *118*, 7288–7295.

(66) Doshi, D. A.; Watkins, E. B.; Israelachvili, J. N.; Majewski, J. Reduced water density at hydrophobic surfaces: Effect of dissolved gases. *Proceedings of the National Academy of Sciences* **2005**, *102*, 9458–9462.

(67) Guardia, E.; Martí, J.; García-Tarrés, L.; Laria, D. A molecular dynamics simulation study of hydrogen bonding in aqueous ionic solutions. *Journal of Molecular Liquids* **2005**, *117*, 63–67.

(68) Knippenberg, M. T.; Mikulski, P. T.; Dunlap, B. I.; Harrison, J. A. Atomic contributions to friction and load for tip–self-assembled monolayers interactions. *Physical Review B* **2008**, *78*, 235409.

(69) Wu, C.-D.; Lin, J.-F.; Fang, T.-H. Molecular dynamic simulation and characterization of self-assembled monolayer under sliding friction. *Computational materials science* **2007**, *39*, 808–816.

Graphical TOC Entry